ARMY RESEARCH LABORATORY

Boundary Integral Technique for Explosion Bubble Collapse Analysis

Stephen A. Wilkerson

ARL-TR-184 August 1993

NOTICES

Destroy this report when it is no longer needed. DO NOT return it to the originator.

Additional copies of this report may be obtained from the National Technical Information Service, U.S. Department of Commerce, 5285 Port Royal Road, Springfield, VA 22161.

The findings of this report are not to be construed as an official Department of the Army position, unless so designated by other authorized documents.

The use of trade names or manufacturers' names in this report does not constitute indorsement of any commercial product.

REPORT DOCUMENTATION PAGE

Form Approved
OMB No 0704-0188

1. AGENCY USE ONLY (Leave blank)	2. REPORT DATE	3. REPORT TYPE AND DATES COVERED
	August 1993	Final, November 1987–January 1988

4. TITLE AND SUBTITLE

Boundary Integral Technique for Explosion Bubble Collapse Analysis

5. FUNDING NUMBERS

RJ14W27

6. AUTHOR(S)

Stephen A. Wilkerson

7. PERFORMING ORGANIZATION NAME(S) AND ADDRESS(ES)

U.S. Army Research Laboratory
ATTN: AMSRL-WT-PD
Aberdeen Proving Ground, MD 21005-5066
Silver Spring, MD 20903-5000

8. PERFORMING ORGANIZATION REPORT NUMBER

9. SPONSORING / MONITORING AGENCY NAME(S) AND ADDRESS(ES)

U.S. Army Research Laboratory
ATTN: AMSRL-OP-CI-B (Tech Lib)
Aberdeen Proving Ground, MD 21005-5066

10. SPONSORING / MONITORING AGENCY REPORT NUMBER

ARL-TR-184

11. SUPPLEMENTARY NOTES

This work was performed under the auspices of the Naval Surface Warfare Center's long-term study program.

12a. DISTRIBUTION / AVAILABILITY STATEMENT

Approved for public release; distribution is unlimited.

12b. DISTRIBUTION CODE

13. ABSTRACT *(Maximum 200 words)*

The dynamics of an underwater explosion bubble, including its collapse and interaction with a free or hard surface, are analyzed using incompressible flow theory and a boundary integral formulation. The formulation of the solution method and the crux of the numerical treatment are presented in detail. A computer program for axisymmetrical problems has been successfully developed. Numerical results, including bubble periods, maximum radii, and velocities of the reentrant jet tip, are compared to available experimental data and to computational results obtained using the PISCES finite difference code.

14. SUBJECT TERMS	15. NUMBER OF PAGES
boundary integral technique; bubble jetting; explosion bubble collapse; PISCES code; explosion bubbles; cavitation; finite element analysis	46
	16. PRICE CODE

17. SECURITY CLASSIFICATION OF REPORT	18. SECURITY CLASSIFICATION OF THIS PAGE	19. SECURITY CLASSIFICATION OF ABSTRACT	20. LIMITATION OF ABSTRACT
UNCLASSIFIED	UNCLASSIFIED	UNCLASSIFIED	UL

INTENTIONALLY LEFT BLANK.

FOREWORD

This work was sponsored under the auspices of the Naval Surface Warfare Center's long-term study program. This program allows employees the opportunity of continued academic study for the period of 1 year. The study was conducted during the summer and fall of 1987 under the aforementioned program. The purpose of this study was to develop an analytical approach for the prediction of underwater bubble collapse and its interaction with the free surface or a solid surface. The report describes the solutions for axisymmetric problems. The approach is shown to be in good agreement with available experimental data and other analytical approaches.

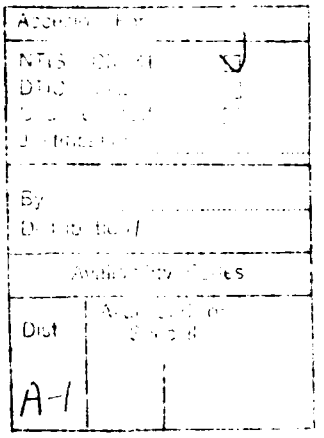

INTENTIONALLY LEFT BLANK.

ACKNOWLEDGMENT

The author gratefully acknowledges the advice, patience, and expertise of Dr. A. Prosperetti, Department of Mechanics, The Johns Hopkins University, Baltimore, MD, who provided the technical foundation of this work. The author would like to give recognition to Mr. K. Kiddy who provided the PISCES analysis included in this work. The author also acknowledges the support of the U.S. Army Ballistic Research Laboratory (BRL), Aberdeen Proving Ground, MD, in making the preparation of this manuscript possible.

INTENTIONALLY LEFT BLANK.

TABLE OF CONTENTS

INTENTIONALLY LEFT BLANK.

LIST OF FIGURES

INTENTIONALLY LEFT BLANK.

LIST OF TABLES

INTENTIONALLY LEFT BLANK.

1. INTRODUCTION

An underwater bubble can exhibit dynamic behavior similar to a mass spring system. For an explosion bubble, the initially high internal pressure will drive the surrounding fluid outward at a decreasing rate. Due to the fluid inertia, the bubble will overexpand, dropping its internal pressure to only a small fraction of the surrounding fluid's hydrostatic pressure. Then the bubble will begin to contract at an increasing rate. The contraction is propelled by the fluid's surrounding hydrostatic pressure. This process will continue until the increasing bubble pressure abruptly reverses the process. Thus, the elastic properties of the gas and water provide the conditions for an oscillating system. This process is termed *bubble pulsation*.

During the contraction phase of the bubble pulsation, variations in the surrounding fluid pressure can cause the bubble surface to contract at different rates. These pressure variations can occur due to bubble migration, a nearby object, the natural gradient of pressure with depth in a fluid, and other disturbances. These external pressure variations will cause a higher rate of inward fluid acceleration near a portion of the bubble surface. The portions of the bubble surface near the higher fluid acceleration will form a jet near the end of the contraction phase of the bubble pulsation. This jet can vary greatly in size and momentum, depending on the factors leading to its formation. This phenomenon is termed *bubble jetting*. The primary purpose of this study was the development of analytical techniques that could be used to study bubble pulsation and bubble jetting.

Much of the interest in underwater bubble dynamics has focused on the behavior of cavitation bubbles. Cavitation bubbles have applications affecting military strategy, propeller and turbine blade damage, and underwater acoustics. Collapsing cavitation bubbles can generate tiny regions where temperatures are in the thousands of degrees with tremendous pressures and fl d velocities. A number of authors (Guerri, Lucca, and Prosperetti 1982; Lezzi and Prosperetti 1987; Prosperetti 1982a, 1982b, 1984, 1986, 1987; Prosperetti, Crum, and Commander 1988; Prosperetti and Jones 1984; Prosperetti and Lezzi 1986; Chahine 1982, 1977; Chahine and Bovis 1983; Chahine and Genoux 1983; Chahine, Genoux, and Liu 1984; Chahine and Sivian 1985; Genoux and Chahine 1984; Johnson et al.; Taib 1985; Chapman and Plesset 1970, 1972) have demonstrated that, in some instances, bubble behavior can be accurately predicted with good accuracy utilizing numerical methods.

The focus of this numeric study is the dynamic expansion and collapse of large bubbles, such as those created by an underwater explosion in the free field, in the vicinity of a free surface, and near a solid body. Bubble collapse is influenced by a number of physical factors. The factors include the gradient of hydrostatic pressure as a function of depth, bubble migration, and a bubble's proximity to nearby solid bodies.

The effect of the pressure gradient on jetting is far more influential for a large bubble than a cavitation bubble. In the former case, the hydrostatic pressure at the bottom of the bubble surface can be twice as high as the hydrostatic pressure at the top of the bubble. Contrarily, bubble migration leads to bubble jetting in both large and small bubbles. In general, bubbles are driven upward by their own buoyancy force. Consequently, the higher velocity of the flow at the head of the bubble leads to a reduction in hydrostatic pressure, while the stagnant flow along the lower surface of the bubble leads to an increase in the hydrostatic pressure. This phenomenon, accompanied by the dynamic collapse of the bubble, will typically yield a bubble jet near the end of the bubble collapse phase. Further, the proximity of the bubble to a solid boundary can also greatly influence the bubble jetting behavior (Figure 1). When a bubble pulsates near a body, the fluid near the object must move faster than the fluid around other portions of the bubble. The result is a decrease in the fluid's pressure near the boundary. This pressure drop in the fluid near the body will generate bubble migration toward the body. When the bubble comes in contact with the body during the expansion phase of its period, the bubble can have a very high water velocity. This is in part due to the dynamic nature of the bubble growth. As the bubble expands, the internal pressure can drop to only a small fraction of the normal hydrostatic pressure in the surrounding fluid field. The result is the jetting of the bubble's lower surface into the body. Finally, the combination of the various effects influencing bubble collapse and jetting can act in conjunction with one another to increase jetting or oppose one another to reduce jetting. The present method described in this report allows the opportunity for these behaviors to be studied separately or in combination with one another.

The present study utilizes an axisymmetric boundary integral formulation which has application for a variety of geometric configurations. The method is computationally efficient due to its dependence on only the boundaries' value for the velocity, the potential, and the potential's first derivative. This approach avoids the necessity of solving Laplace's equation in the entire domain occupied by the

liquid which would be computationally intensive. The resulting range in computation time can vary from minutes for free field calculations, to less than one-half hour for computations involving free surfaces or a boundary. The computational device serving as a basis for these comparisons is the VAX 8800. To illustrate the performance and accuracy of the method, a number of comparisons were made. These comparisons included: exact vs. predicted solutions for spherical bubbles; experimental bubble radii and period comparisons; and bubble jet tip velocities vs. compressible flow theory calculations using the hydrocode PISCES. In these cases, the method is shown to be in good agreement with available data. Further, a number of calculations very near the free surface are performed showing the idealized formation of the water spray dome. Using this free surface calculation, the limitations of the methodology are discussed.

The growth and collapse of large bubbles, such as those created by underwater explosions near nonaxisymmetric underwater structures, are also of interest. In this scenario, the combination of gravity-induced collapse and collapse caused by migration and proximity to nearby structures can result in extremely high velocities of the bubble reentry jet tip. Analysis of bubble-structure interaction is generally three-dimensional in nature due to the effects of gravity and the orientation of the structure. Solution of this problem is briefly discussed in Section 2.

2. MATHEMATICAL FORMULATION

In this mathematical formulation model, the flow induced by one or more bubbles is considered. The fluid occupies a domain Ω bounded by the bubble surfaces, S_b, solid boundaries, S_r, and a surface at infinity, S_∞ (Figure 2). The fluid, contained in domain Ω, is considered incompressible and inviscid.

In the case of underwater explosive detonations, a chemical reaction converts the original material into a gas at very high temperatures and pressures. The temperatures can be of order 3,000° C with pressures of order 50,000 atm (Landau and Lifshitz 1959). The result of the initial detonation is a compression or shock wave being emitted into the fluid field, followed by the dynamic expansion and contraction of the gas bubble. After the release of the shock wave, which is an early time phenomenon, the speed of the bubble surface remains an order of magnitude smaller than the speed of sound in water. Therefore, imposing an incompressibility condition on the fluid is deemed valid for this flow condition.

Using the bubble radius as a characteristic length in the expansion or contraction phase of the bubble pulse, a Reynolds number can be calculated. The Reynolds number for an underwater explosion is found to be high through most of the bubble growth and collapse. Recalling that the Reynolds number is a ratio of inertial to viscous forces, it is clear that neglecting viscid terms in the conservation of momentum equation detracts very little from the problem solution. Furthermore, under the assumption that the flow is inviscid and irrotational flow, the velocity field can be found from the gradient of a potential. In the case of a cavitation bubble, similar assumptions were shown to be valid by Guerri, Lucca and Prosperetti (1982).

The mathematical problem described above can be stated in the following form. The divergence of the velocity vector is zero for an incompressible fluid. This expression is found from the conservation of mass equation and can be written as

$$\nabla \cdot \underline{u} = 0. \tag{1}$$

For irrotational flow, the curl of the velocity vector is zero and can be written as

$$\nabla \times \underline{u} = 0. \tag{2}$$

This expression is also satisfied when the velocity $\underline{u}$ equals the gradient of a potential which is

$$\underline{u} = \nabla\phi. \tag{3}$$

Combining Equations 1 and 3 yields Laplace's equation. Laplace's equation is satisfied in the domain Ω occupied by the fluid and can be written in terms of the potential as

$$\nabla^2\phi = 0. \tag{4}$$

The boundary conditions necessary for the solution of Laplace's equation in the domain Ω can be stated as

$$\frac{dx}{dt} = \nabla\phi \quad \text{on } S_b \tag{5}$$

$$\phi \rightarrow 0 \; P \rightarrow P_\infty \quad \text{at } S_\infty \tag{6}$$

with

$$\frac{\partial \phi}{\partial n} = \nabla \phi \cdot n = 0 \quad \text{on } S_b, \tag{7}$$

where $\underline{x}$ is the distance to the boundary from a consistent point of reference.

The conservation of momentum, or Navier Stokes equation under the assumption of incompressible fluid and irrotational flow, can be written in the form

$$\frac{D\underline{u}}{Dt} = \frac{-\nabla P}{\rho} + g, \tag{8}$$

where $D\underline{u}$ represents the total derivative, P the pressure, ρ the density, and g the gravity. Using the identity:

$$\underline{u} \cdot \nabla \underline{u} = \frac{\nabla \underline{u}^2}{2} - \underline{u} \times \nabla \times \underline{u} \tag{9}$$

and the relations in Equations 2 and 3, the equation for conservation of momentum reduces to the form given by Euler (Landau and Lifshitz 1959) as

$$\frac{\partial \phi}{\partial t} + \frac{\underline{u}^2}{2} + \left[\frac{P_\infty - P_R}{\rho}\right] + gz \tag{10}$$

with P_R representing the pressure on the surface of the bubble and P_∞ the pressure at infinity. The pressure P_∞ can be determined by the choice of a reference point. For example, if the point of reference at infinity is the free surface of the water, P_∞ = 1 atm and z is the depth of the bubble segment. P_R can be found from the adiabatic pressure balance equation given by Cole (1948) as

$$P_R = 7.8\left[\frac{W}{V}\right]^{\gamma} + \sigma \tag{11}$$

where W is the weight of the explosive in grams of TNT equivalent, V is the volume in centimeters cubed, and the pressure, P_R, is given in kilobars. The σ term is added to account for the effects of surface tension. For a cavitation bubble, a similar adiabatic expression can be used.

The formulation strategy for the time integration of the equation of motion is straightforward. If the bubble surface S_b, internal pressure, and the value of the potential and its first derivative on the bubble surface are known, Equations 7 and 10 can be solved while marching through time. In order to solve for the potential's first derivative on the bubble surface, Laplace's equation (Equation 4) must be solved. This can be accomplished using the boundary conditions given in Equations 5, 6, and 7 and using a boundary integral method. The starting point of this solution to Laplace's equation makes use of Green's second identity which is

$$\int_V \left[\phi \nabla^2 \psi - \psi \nabla^2 \phi\right] dV = \int_S \left[\phi \nabla \psi \cdot n - \psi \nabla \phi \cdot n\right] dS \tag{12}$$

with ψ being a function of choice. The V represents integration over the volume and S represents integration over the surface. The most obvious choice for ψ is

$$\psi = \frac{1}{|\underline{x} - \underline{x}|} \tag{13}$$

which is the solution of the Poisson's equation having the form

$$\nabla^2 \psi = -4\pi\delta(\underline{x} - \underline{x}) \tag{14}$$

where $\underline{x}$ and $\underline{x}$ are the reference and current coordinates of the bubble surface (Figure 3). The choice of Poisson's equation and the Dirac function are ideal because the remaining volume integral given on the left-hand side of Equation 12 reduces to a constant along each bubble segment.

With the substitution of Equations 4, 13, and 14 into Equation 12, the formulation reduces to a surface integral with the following form:

$$2\pi\phi(\underline{x}) = \int_S [\phi \nabla\psi \cdot n - \psi \nabla\phi \cdot n] dS. \tag{15}$$

The factor of 1/2 in the left-hand side of the integration in Equation 15 arises from the fact that the integration on the bubble boundary can only be carried out around half the point of reference which is the portion in the domain Ω.

Equation 15 applies to both three-dimensional developments and the present axisymmetric formulation. The three-dimensional approach can be accomplished using first-order and second-order quadrilateral or triangular finite element techniques. The resulting integration would proceed in much the same way as in the axisymmetric case. However, the biggest difference in the three-dimensional solution is in the computation times required to solve problems. The computation time for the three-dimensional case would undoubtedly be an order of magnitude higher than the axisymmetric formulation. Therefore, the present axisymmetric formulation affords some basic advantages in the study of bubble jetting phenomena. The real drawback is the inability of the present method to tackle more complex interactions of bubbles and various underwater objects such as cylindrical and spherical bodies in nonaxisymmetric orientations.

The axisymmetric formulation begins by a suitable choice of coordinate systems. The choice of the cylindrical coordinate system for this case will reduce the integration around the bubble surface to an elliptic integral. Using cylindrical coordinates, we can write the following:

$$\underline{x} = (r\cos\theta,\ r\sin\theta, \zeta) \tag{16}$$

for the reference coordinate system and

$$\underline{x} = (R, O, Z) \tag{17}$$

for our current coordinate system. Substitution of these cylindrical coordinates into Equation 15 and the rearrangement of terms reduced the integration to the following form:

$$\frac{1}{2\pi}\int_\Gamma r\frac{\partial\phi}{\partial n}\int_0^{2\pi}\frac{d\theta}{|\underline{x}-\underline{x}|}d\Gamma = \phi(\underline{x}) + \frac{1}{2\pi}\int_\Gamma r\frac{\partial}{\partial n}\int_0^{2\pi}\frac{d\theta}{|\underline{x}-\underline{x}|}d\Gamma \tag{18}$$

where $d\Gamma$ represents the integral on a surface element (Figure 3) and θ the angle around the bubble circumference. The integral about $d\theta$ can be reduced to an elliptic integral of the first kind with a fair amount of algebraic manipulations. The elliptical integral introduces a logarithmic term which is singular for the cases when the current coordinate and the reference coordinate coincide. The resulting singularity in the integration is bounded and occurs due to the use of the Dirac delta function. An accurate calculation of this singularity will result in a more stable and accurate bubble model. After experimentation with various expansions, a Gaussian quadrature with weight log (ξ) was found to give the best results (Wilkerson 1987). The quadrature allowed the estimation of error within acceptable limits. The final form of the integration can be written as

$$\frac{1}{2\pi}\frac{\partial\phi}{\partial n}\int_\Gamma G(\underline{x},\underline{x})\,d\Gamma = \phi(\underline{x}) + \frac{1}{2\pi}\phi(\underline{x})\int_\Gamma H(\underline{x},\underline{x})\,d\Gamma \tag{19}$$

where $G(\underline{x}, \underline{x})$ and $H(\underline{x}, \underline{x})$ are functions of the reference and current coordinates and an elliptic integral. Using a straight line approximation for the axisymmetric bubble boundary (Figure 3), the gradient of the potential can be found using the following matrix expression by a Gaussian elimination routine. The basic expression is

$$\sum_{j=1}^{n} a_{ij}\omega_j = b_i \quad i = 1,2,3...n \tag{20}$$

where

$$a_{ij} = \frac{1}{2\pi}\int_{\Gamma_j} G(\underline{x}_j,\underline{x}_i)\,d\Gamma_j \tag{21}$$

$$b_i = \phi(\underline{x}_i) + \sum_{j=1}^{n}\phi(\underline{x}_j)\,\frac{1}{2\pi}\int_{\Gamma_j} H(\underline{x}_j,\underline{x}_i)\,d\Gamma_j \tag{22}$$

and

$$w_j = \frac{\partial \phi}{\partial n} = \text{const.} \tag{23}$$

The solution for $\partial\phi/\partial n$ can now be applied to the conservation of momentum equation and marched through time. The updating of line segments and the momentum equation given in Equation 7 is accomplished with a finite difference time integration scheme and linear interpolation between the nodes. The first-order form of the finite difference formula is

$$\phi_{i+1} = \phi_i + \left\{ \frac{\mu^2}{2} + \left[\frac{P_\infty - P_R}{\rho} \right] + gz \right\} \Delta t. \tag{24}$$

However, higher order formulations, depending on multiple values of the potential, are used after the initial time step. A similar expression is used to update the geometry. These higher order formulations do not increase computation time significantly. The majority of the computation time needed in the calculation is spent doing the integrations in Equation 19 and assembling and solving the matrix formulation given in Equation 20. Therefore, the contributing factors influencing computation time are the number of segments and the number of time steps. The amount of line segments determines the total number of integrations in a time step and also the size of the matrix (Equation 20) that must be solved. For the free field cases, 32 line segments were found to be sufficient. However, in the cases involving the free surface or a solid surface, 84 line segments were used. No attempt to optimize the method was made in the present study. Contrarily, the effect of time step size was investigated. In the free field cases, any time step less than 1/450th of the total bubble period was found to cause problems at the beginning and at the end of the bubble period. This is probably due to the relative speed of the individual line segments during these phases of the bubble oscillation period. A formulation involving a variable-sized time step dependent on the highest speed of a segment would probably result in greatly reduced computation times. For the present, the author's primary concern was with the validation and accuracy of the methodology and with exploration of the limitations of this formulation. Consequently, a 1/1,000th of the bubble total period was used in all cases examined. The bubble period was estimated using standard empirical rules (Swift and Decius 1950) for underwater explosive detonations.

3. RESULTS

The validation of this methodology was initiated by attempting to solve simplistic problems. The problems were gradually changed to include more complex phenomena such as bubble interactions with the free surface and solid bodies. The problems and limitations are discussed with possible solutions extending the method. What follows is a discussion of various problem types, the limitations of the current approach, and possible advantages in the present methodology.

The starting point of the validation was a comparison of the boundary integral method to the exact solution for a spherically symmetric bubble model. The conservation of momentum equation given in Equation 10 was modified to exclude gravity. With gravity removed and in the absence of other bodies, the solution technique should duplicate the exact formulation for a spherically symmetric model. The conservation of momentum equation under spherical symmetry and the conservation of mass equation can be integrated to yield

$$\dot{R}^2 = \left[\frac{R_o}{R}\right]^3 \dot{R}_o^2 + \left[\frac{2}{3}\right]\left[\frac{P_R - P_\infty}{\rho}\right]\left\{1 - \left[\frac{R_o}{R}\right]^3\right\} \tag{25}$$

where $\dot{R}$ represents the current velocity of the bubble surface; R the current radius; and P_R, P_∞, and ρ (as given in Section 2) are the internal bubble pressure, reference pressure, and fluid density. The subscript o represents the referenced values. Using the boundary integral method for R, R_o, and $\dot{R}_o$, the estimated value for $\dot{R}$ was compared to the exact solution given by Equation 25. In both bubble expansion and bubble contraction, the boundary integral method approached the exact solution, or the limit of the methods accuracy. The accuracy of the method appeared to improve with time. This is caused by the potential's initial condition being assumed zero. Therefore, the method requires a number of steps to calculate a reasonable value for the potential. Furthermore, this assumption is particularly good in the case of an underwater explosion where the internal pressure is large by comparison to the external pressure. The result is that the early bubble motion is dominated by the large pressure differential, thus allowing the method to retain good overall accuracy under the zero initial potential assumption. This accuracy is shown for both a first-order finite difference integrator and a second-order time integrator in Tables 1 and 2, respectively.

The convergence seen in Tables 1 and 2 occurs for two reasons. First, the assumption allowing the potential to be zero initially will require a few time steps to achieve a reasonable level of equilibrium. This error will decrease rapidly at first then gradually thereafter. The second reason for continued convergence is the constant reduction in pressure difference as the bubble volume grows. This reduction in pressure difference results in a decrease in the radial velocity of the bubble. Slower velocities under a constant time step are attributed to increased convergence. To estimate the effects of bubble radial velocity on convergence, the method was used with a constant time step under constant pressure. The constant pressure will result in a constantly increasing radial velocity. This should allow an estimation of the error attributed in time step size vs. bubble radial velocity. The results are summarized in Tables 3 and 4.

The results showed that, for a constant time step of .01 and velocities sufficiently low, the convergence and accuracy were quite reasonable. However, if the bubble were allowed to iterate long enough, or if the pressure differential was increased, the convergence reached a minimum and then began to diverge in accordance with bubble radial velocity. By comparing Tables 1 and 2 to Tables 3 and 4, the error effects of a particular time step at a given velocity can be seen. In Tables 1 and 2, the time step used was .001 for velocities of order 102, while Tables 3 and 4 have a time step of .01 for speeds of order 100. As expected, Tables 3 and 4, which have a smaller velocity vs. time step ratio, converge faster to a reasonable error. In as much as the solutions converged to reasonable values in both cases, it indicated that the initial conditions resulted in a reasonable cumulative error. The issue of time step size seems to be the most crucial aspect in keeping the cumulative error to a minimum. This became particularly important for bubble jetting where the velocities were as high as 1,000 ft/s for the bubble segments near the nose of the reentrant jet tip. These high velocities lead to numerical instabilities which would stop the analysis. Therefore, the bubble maximum velocities were compared to the bubble period so that a rule of thumb could be developed for the time step. It was found that a time step of 1/1,000th of the bubble period would give reasonable results in all cases investigated. A further analysis of the time step could lead to a variable step size dependent on only the maximum speed of the fastest bubble segment. However, no attempt to find a suitable ratio of time step to segment velocity has been made.

The second phase of the validation was to compare bubble periods and maximum bubble radius to experimental results. Swift and Decius (1950) offered data for an abundant variety of explosive sizes

Table 1. Bubble Exact vs. Calculated Variable Pressure (First-Order Time Integration)

Time Step	Radial Velocity		Error (%)
	Exact	Calculated	
10	51.24	53.10	3.6
20	33.68	33.77	0.25
30	25.42	25.37	0.19
40	8.19	8.18	—

Table 2. Bubble Exact vs. Calculated Variable Pressure (Second-Order Time Integration)

Time Step	Radial Velocity		Error (%)
	Exact	Calculated	
10	58.04	56.67	2.4
20	34.93	34.94	0.02
30	25.97	25.97	—

Table 3. Bubble Exact vs. Calculated Constant Pressure (First-Order Time Integration)

Time Step	Radial Velocity		Error (%)
	Exact	Calculated	
10	0.09091	0.09036	0.60
20	0.1944	0.1943	0.046
30	0.3067	0.3066	0.012

Table 4. Bubble Exact vs. Calculated Constant Pressure (Second-Order Time Integration)

Time Step	Radial Velocity		Error (%)
	Exact	Calculated	
10	0.0999	0.1004	0.48
20	0.2048	0.2047	0.06
30	0.3177	0.3177	—

and depths to be attempted. A number of the shots presented in the Swift report were selected at random and compared to the solution technique presented in this report. The results are presented in Tables 5 and 6. The results generated in Table 5 are of greater importance because the methods used to record bubble period are more accurate than maximum bubble radius data. The accuracy stems from the use of piezoelectric gauges which can record the pressure waves emitted initially and with each successive bubble pulse. The initial shock wave indicated the beginning of the period and the first bubble pulse, which occurs just after bubble minimum, indicates the end of the period. Due to the high speed of sound in water, the method gives very accurate results. For the data compared in Table 5, the analytical method gives reasonable results.

On the contrary, the maximum bubble radii data for the Swift report was not as accurate. These data were obtained from measurements taken from simultaneous photographic records. As Swift and Decius (1950) pointed out, the relative narrow angle of view from the high-speed cameras and the problems with distortion and lighting made it difficult to make bubble radii measurements better than 2–4%. Further, depth measurements were obtained from a weighted line which could vary slightly due to ocean currents. These factors are attributed to a loss of accuracy in the bubble radii comparisons shown in Table 6.

The accuracy of the method was summarized by making a number of radius vs. time plots in comparing computational values to those found in the Swift and Decius (1950) report. These plots are given in Figures 4–9. The plots follow the growth and decay profiles of the bubble first period quite well. These plots represent results generated by tests involving a number of charge weights at varying depths.

Table 5. Bubble Period (Calculated vs. Experiment)

Shot No.	Charge Weight (lb)	Charge Dept (ft)	Period (ms)	Calculated (ms)	Error (%)
G1F	0.651	343.	27.40	26.40	1.9
G2F	0.660	304.	29.80	29.76	0.13
G5F	0.662	305.	29.89	29.70	0.64
G6F	0.658	304.	29.92	29.73	0.64
G7F	0.669	298.	30.23	30.39	0.50
G8F	0.663	304.	29.82	29.80	0.0
G9F	0.651	304.	29.64	29.62	0.0
G17F	0.660	305.	29.62	29.68	0.20
G18F	0.660	302.	29.61	29.92	1.0
G20F	0.660	538.	19.64	18.90	3.7
G21F	0.651	539.	19.10	17.50	9.0
G23F	0.658	567.	18.14	18.30	0.88
G70F	0.660	503.	19.90	20.00	10.50
G71F	0.658	463.	21.00	21.40	1.90
G72F	0.660	586.	17.85	17.80	0.30
G73F	0.655	576.	18.16	18.00	0.90
G74F	0.660	556.	18.10	18.60	2.80
G76F	0.660	587.	17.10	17.38	0.30

AVERAGE 1.0%

Table 6. Bubble Period (Calculated vs. Experiment)

Shot No.	Charge Weight (lb)	Charge Dept (ft)	Period (ms)	Calculated (ms)	Error (%)
G1F	0.651	343.	—	17.0	—
G2F	0.660	304.	18.80	18.49	1.68
G5F	0.662	305.	18.80	18.48	1.70
G6F	0.658	304.	18.80	18.47	1.80
G7F	0.669	298.	18.90	18.70	1.0
G8F	0.663	304.	18.90	18.52	2.1
G9F	0.651	304.	18.70	18.40	1.6
G17F	0.660	305.	19.40	18.46	5.1
G18F	0.660	302.	19.40	18.53	4.7
G20F	0.660	538.	15.90	15.00	6.0
G21F	0.651	539.	15.70	14.40	9.0
G23F	0.658	567.	15.61	14.70	6.3
G70F	0.660	503.	—	15.35	—
G71F	0.658	463.	16.60	15.80	4.9
G72F	0.660	586.	15.40	14.50	6.0
G73F	0.655	576.	15.60	14.60	7.0
G74F	0.660	556.	15.70	14.80	6.0
G76F	0.660	587.	15.10	14.50	3.9

AVERAGE 4.0%

The deviations of values obtained from theory found in these figures is approximately of the same magnitude as the errors given in Tables 5 and 6. For deeper shots, a larger error occurs with the radius calculations. This is believed to be caused by a number of factors. As pointed out earlier, the experimental data is not as accurate for radius calculations as it is for the bubble period. Further, the initial conditions seem to play an important role in maximum bubble radius calculations. When the initial radius was decreased, the radius estimates improved. This is due to the increase in hydrostatic pressure at increased depths and the effect it plays on the overall pressure difference. Additionally, the effects of bubble radius calculations are less forgiving for smaller charges than for larger ones. However, in the interest of consistency, all results calculated in this report represent the same initial conditions for internal bubble pressure and the potential on the surface.

All of the data compared thus far represents relatively small charges. Therefore, bubble periods for a 300-lb charge detonated at shallow depths are compared to results presented in Cole (1948). Figure 10 compares the observed periods in Cole vs. those predicted by theory. These calculations include the effects of a free surface in the flow field. For the shallower depths, Figures 11–14 show the growth and collapse of the bubble surface and the effects of the free surface.

When the bubble is closer to the free surface, the effects of the free surface become more evident. This can be seen in Figures 11–13 in terms of bubble migration. The migration is retarded due to its close proximity to the free surface. Figure 14 represents a fictitious scenario. The bubble, in this case, would have undoubtedly broken through the free surface, venting its high-pressure gases. It was not surprising that the calculation for this case became unstable and inadvertently terminated. Therefore, understanding the limitations of the method are important in interpreting the validity of the results. For a bubble at deeper depths, the bubble behavior becomes less influenced by the free surface. At depths greater than 100 ft for the 300-lb explosive, the bubble profile becomes indistinguishable from the free field profile for a similar calculation.

To estimate the accuracy of the method for predicting reentrant water jet tip velocities, a calculation was compared with a PISCES code calculation. The PISCES code has been used for a number of calculations with regard to underwater explosion bubbles, and it is considered reasonably accurate. The comparison for peak reentrant jet velocities was made between the present method and PISCES. If the boundary integral method presented were valid, the two methods should present similar results. As it turned out, the exact time and location of the peak jet velocities varied slightly

the two methods. For the PISCES calculation, the peak velocity occurred just behind the bubble surface and was found to be 1,148 ft/s. A line estimating the location of the bubble surface, with regard to peak velocity, is shown in Figure 15. Since an Euler method has been used in the PISCES calculation, the interface between different materials is not defined exactly. However, an estimated profile is shown in Figure 16. For the incompressible flow calculation, the maximums and minimums for the potential must occur on the boundary to satisfy the uniqueness of Laplace's equation. The highest velocity recorded in the calculation occurred just as the bubble's lower surface broke through the bubble's upper surface (Figure 17). A dotted line estimating the intersection of the two results is shown in Figure 15. The results indicate a reasonable correlation between the two methods. However, a more accurate estimation of the error can only be made through direct comparison with experimental results which are presently unavailable.

A final calculation was performed for an explosion bubble near a solid boundary. The results showing the collapse and upward migration toward the solid boundary are summarized in Figure 18. For this calculation, a 300-lb charge of TNT was detonated 12 m below the solid surface at a depth of 12 m. It is interesting to note the similarities and differences between the free surface calculation of the same weight and depth (Figure 12) and this case. The expansion and overall period of the bubble growth are not disproportionately in disagreement. However, as expected, the solid boundary increases migration toward the boundary while having little effect on the formation of a bubble jet. On the other hand, the free surface condition led to decreased migration and a retardation of bubble jet formation. In general, the free surface condition can lead to bubble blow-out (where the bubble vents through the free surface), bubble downward migration at certain distances from the free surface, and the retardation of bubble jetting. Therefore, it is clear that a nearby structure or solid boundary can lead to bubble jetting into the structure even when near the free surface.

4. SUMMARY

The boundary integral method can be used for the prediction of bubble behavior in a variety of scenarios. While the present study offers only limited results, the method shows promise for future, more in-depth studies. The method shows good agreement with other analytical prediction techniques as well as a variety of experimental data. This report offers the only example of such comparisons found in the literature. The program developed also offers a number of improvements which include efficient programming (under 350 lines of code) and an accurate method for the calculation of the

singularity in the problem. This approach allows the analytical study of bubble pulsation and jetting behavior in coordination with experimentation. Future studies of this nature should include the three-dimensional aspects of bubble collapse, thus bringing the method to its full potential.

In summary, the methodology presented was simple to use, computationally efficient, and reasonably accurate. The overall cost and reliability of the method may prove a valuable aid in guiding and analyzing experimental work.

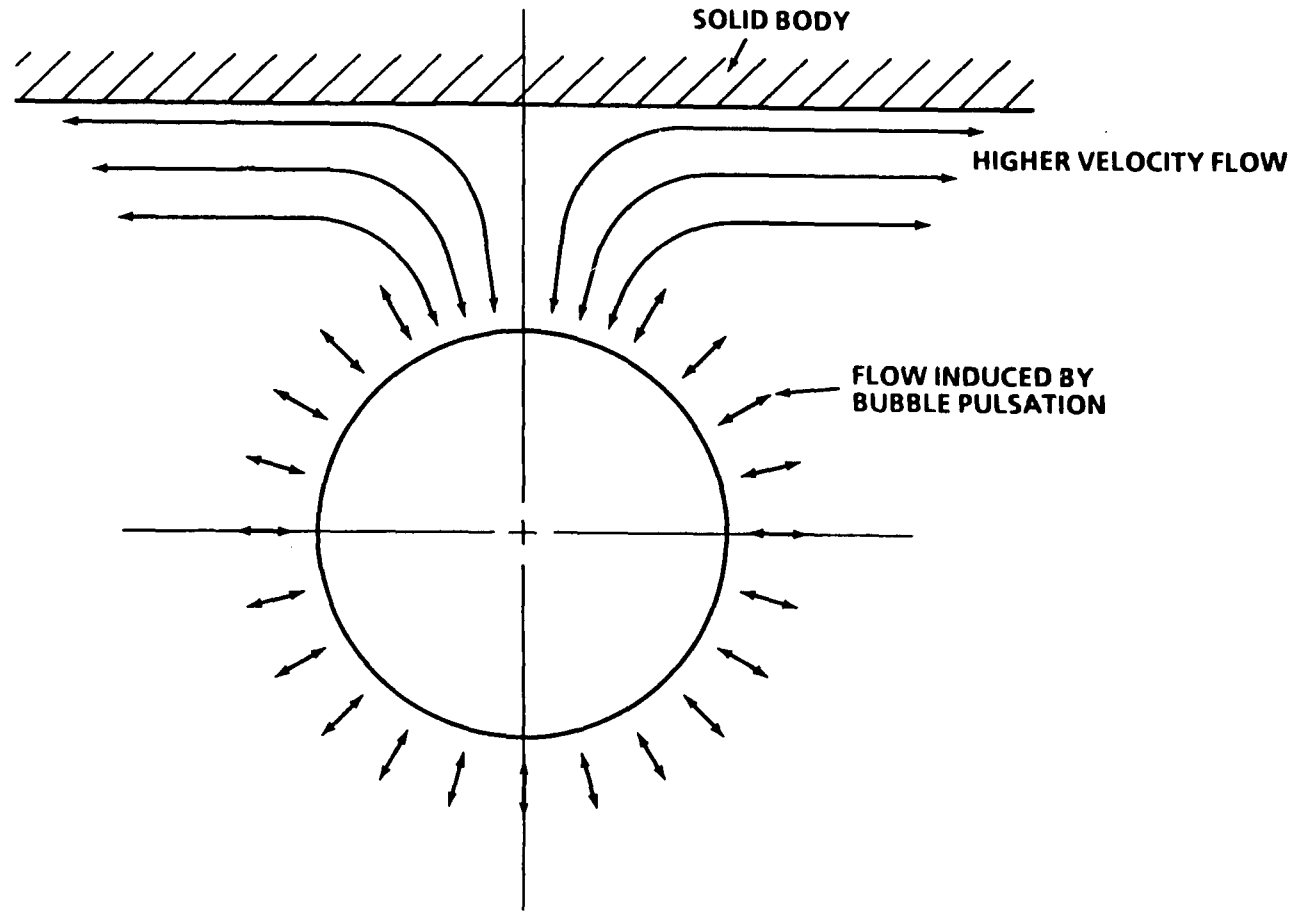

Figure 1. Flow-Induced Migration Near a Boundary.

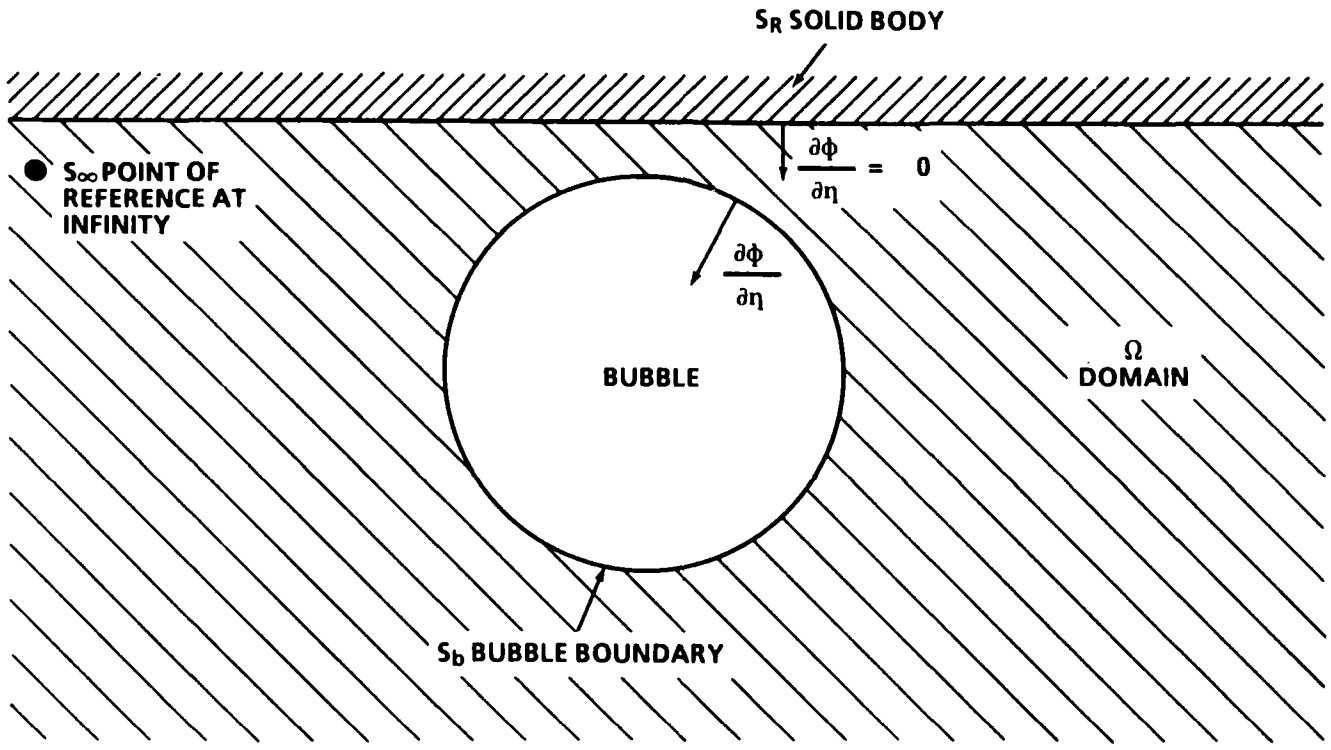

Figure 2. Boundary Conditions.

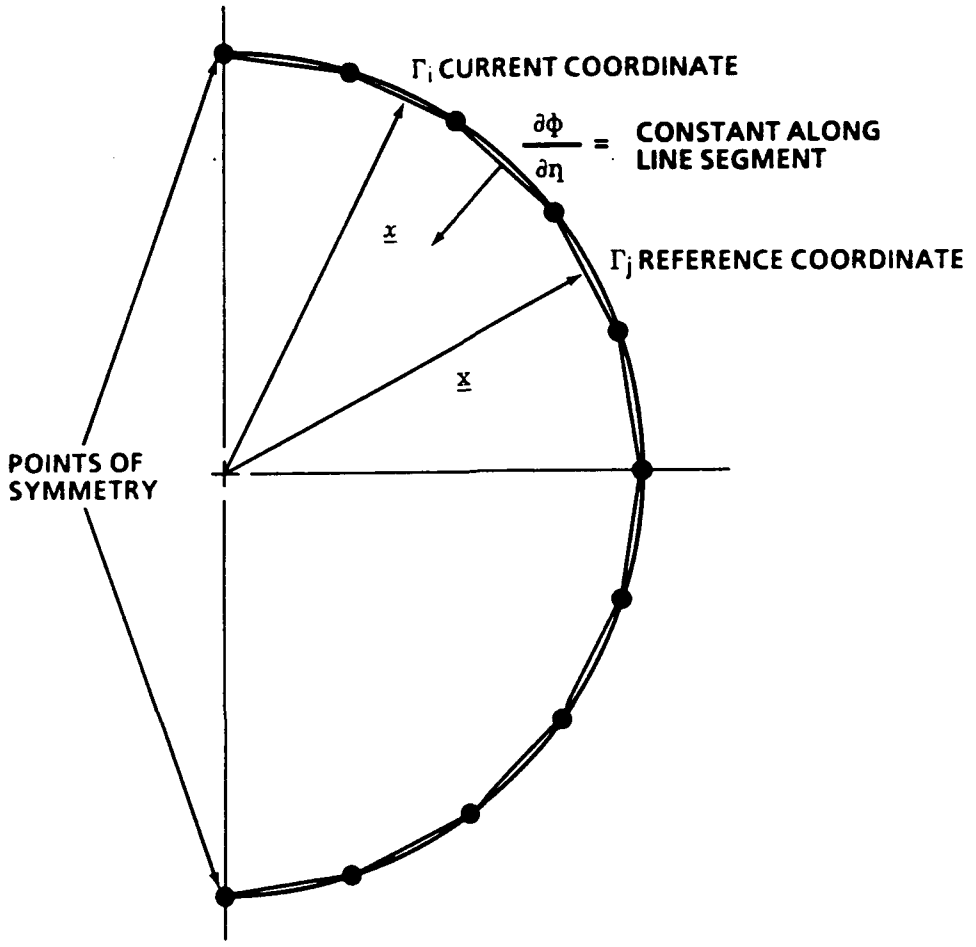

Figure 3. Bubble Partitioning.

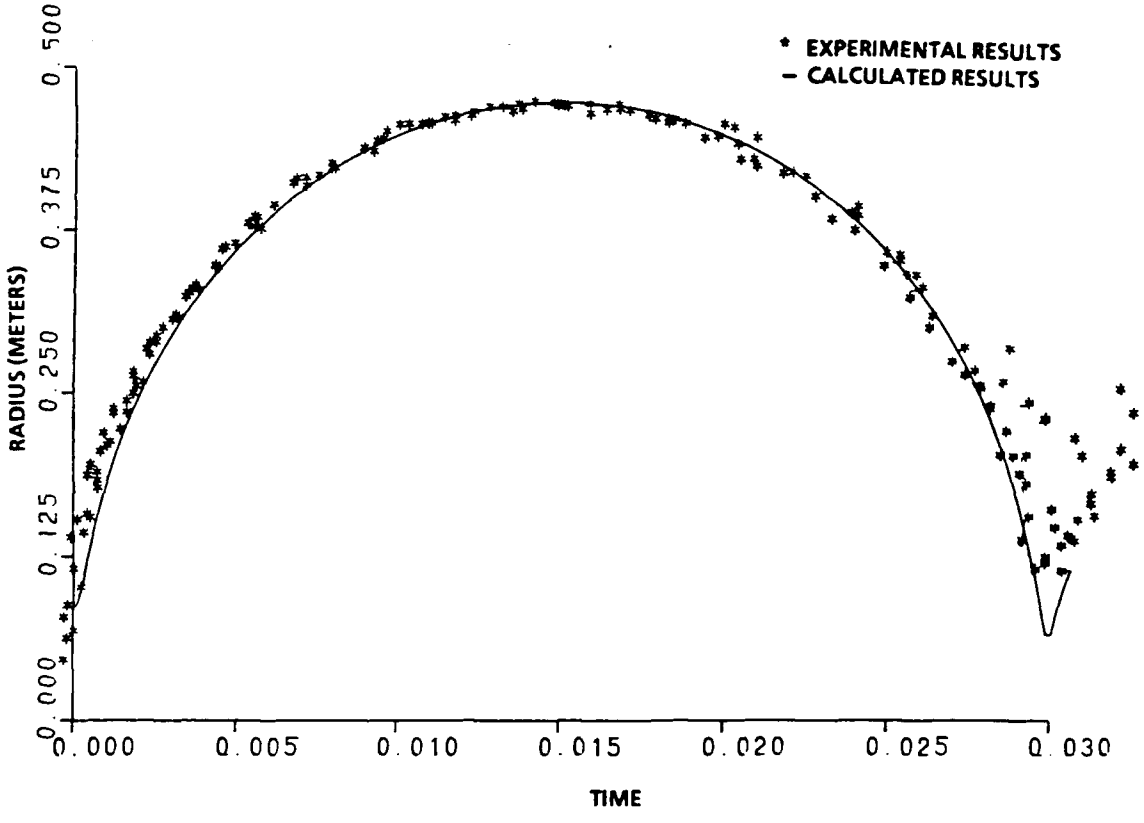

Figure 4. Bubble Radius vs. Time plot (.66 lb TNT 300 ft).

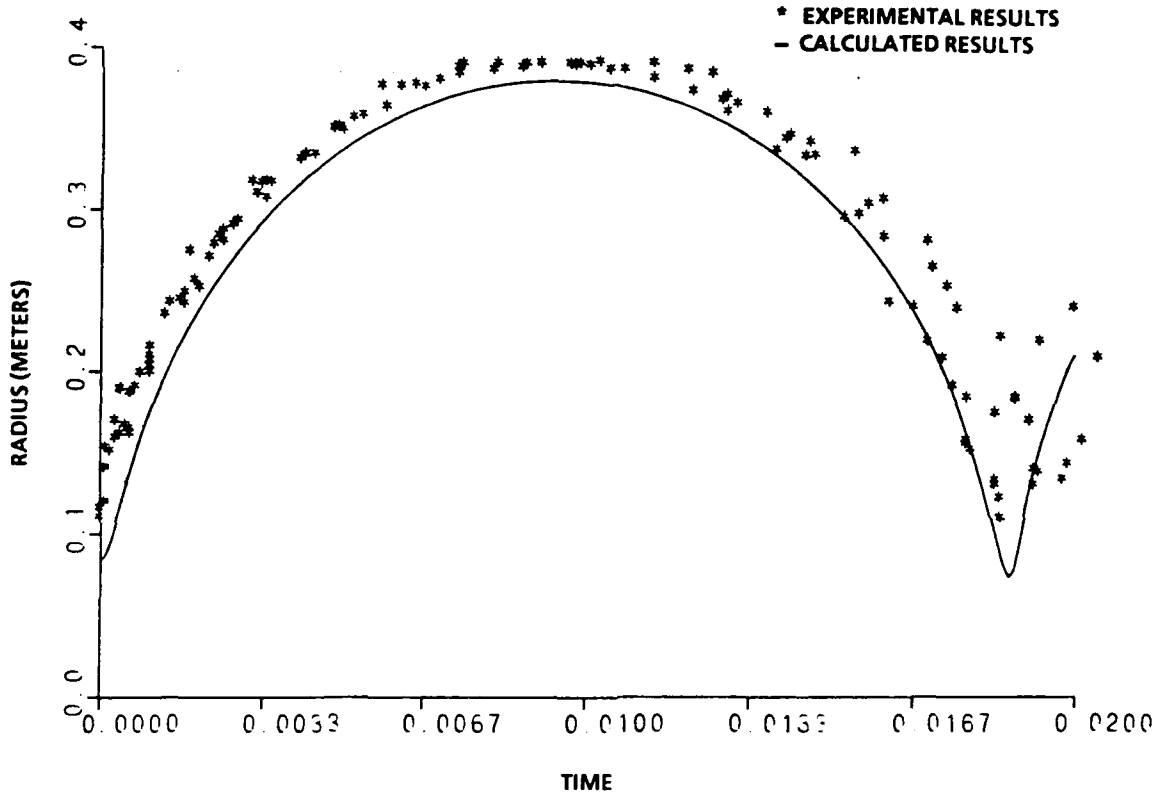

Figure 5. Bubble Radius vs. Time Plot (.66 lb TNT 550 ft).

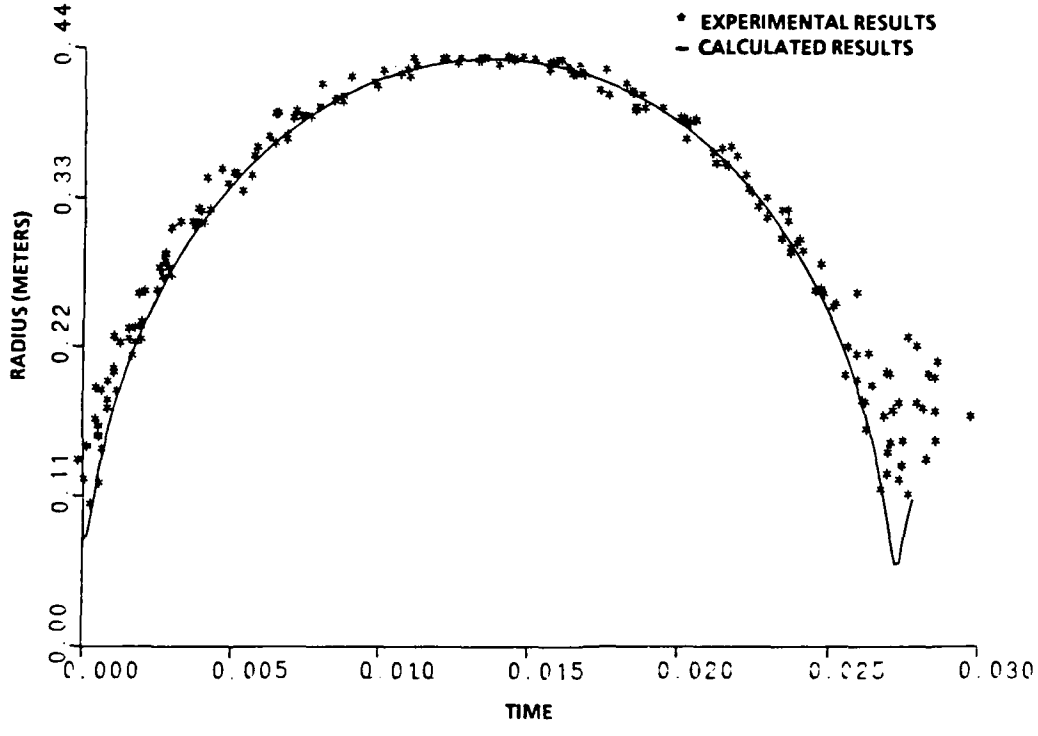

Figure 6. Bubble Radius vs. Time Plot (.5 lb TNT 300 ft).

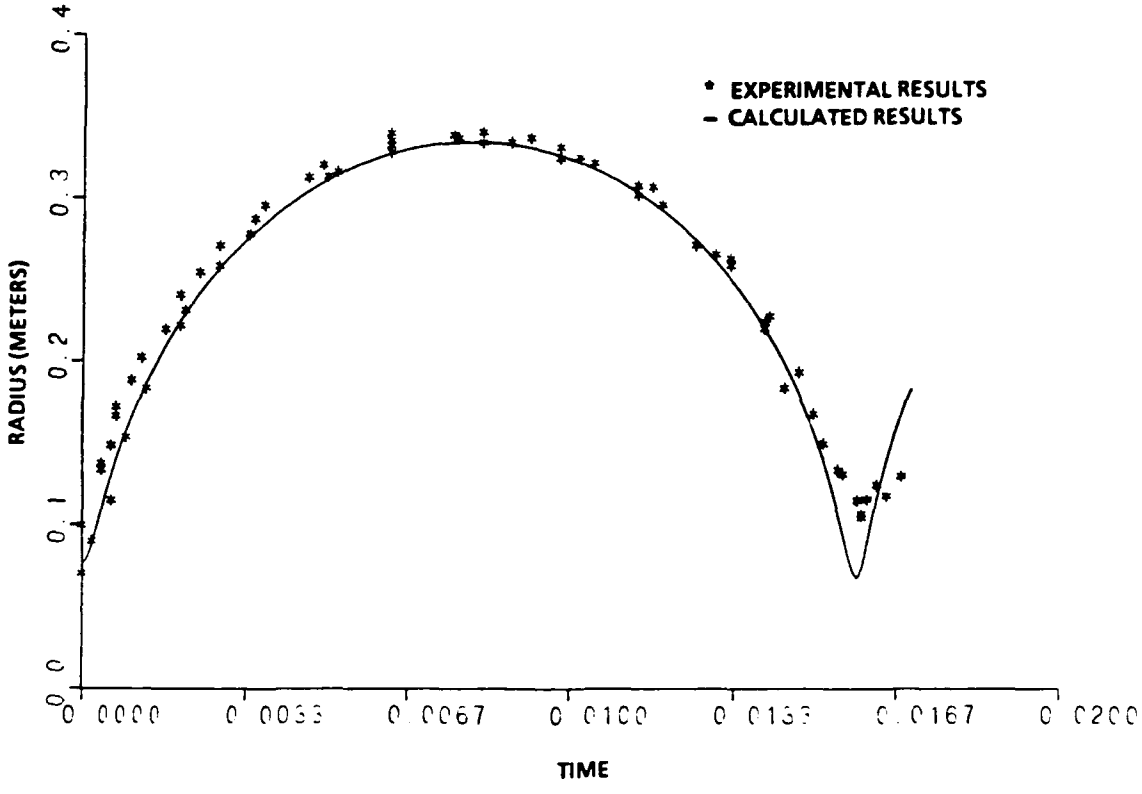

Figure 7. Bubble Radius vs. Time Plot (.5 lb TNT 600 ft).

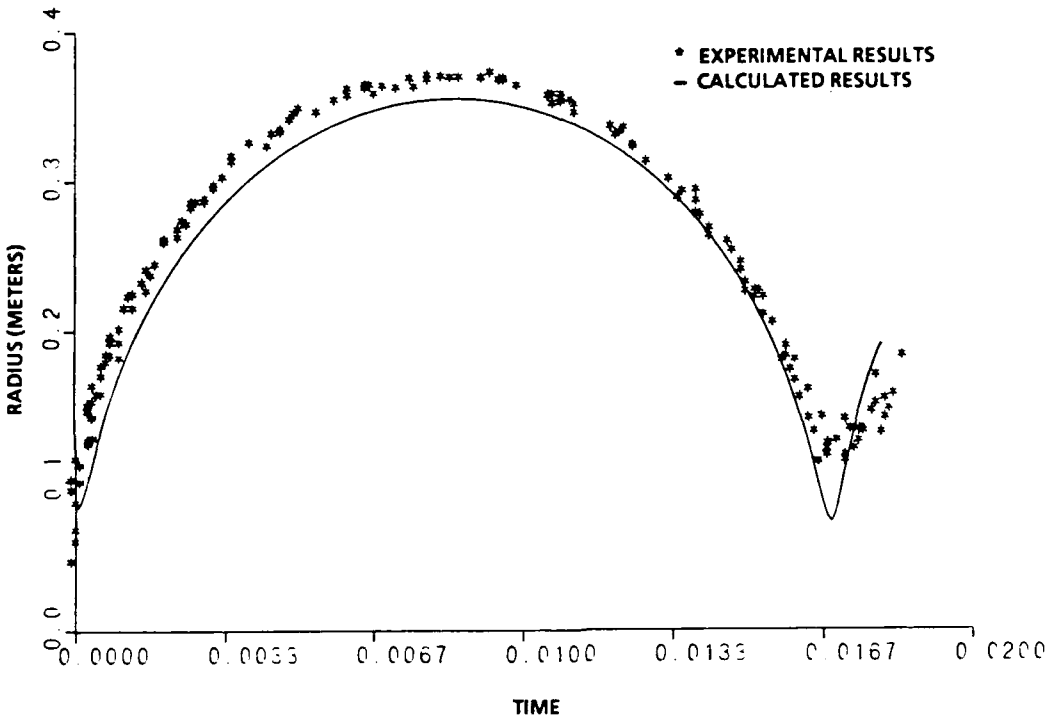

Figure 8. Bubble Radius vs. Time Plot (.6 lb TNT 600 ft).

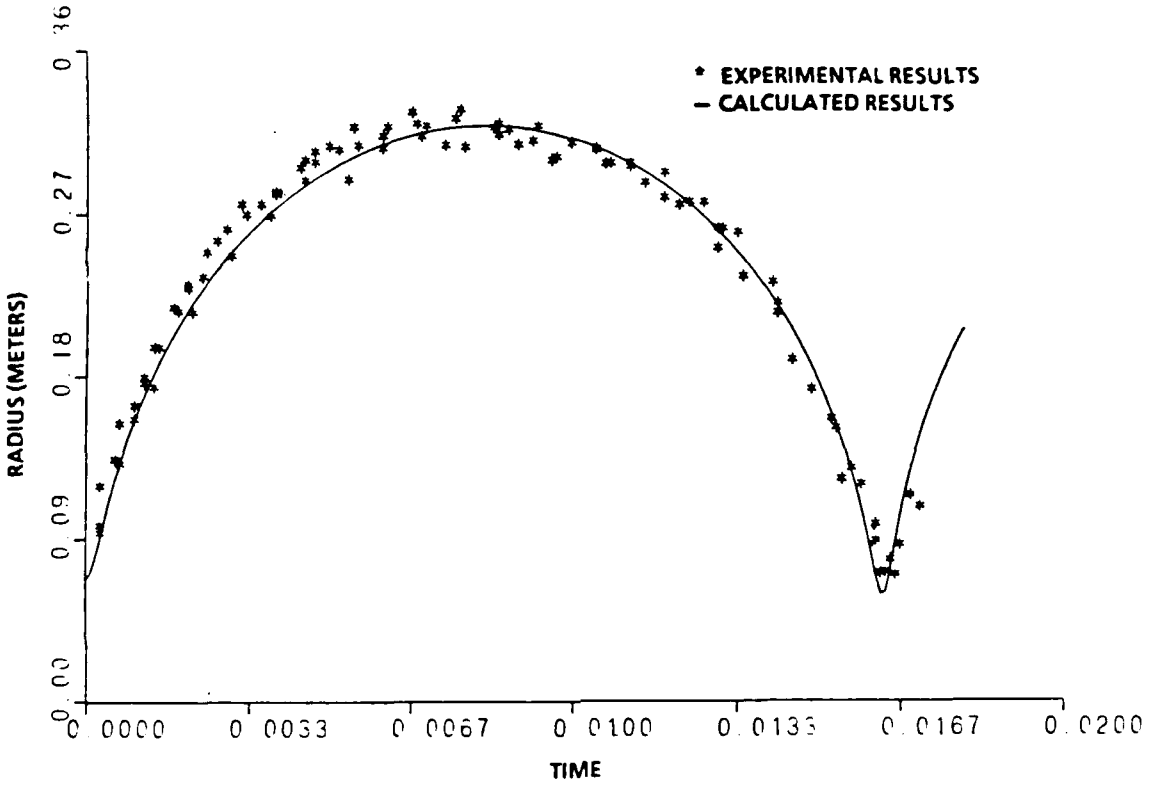

Figure 9. Bubble Radius vs. Time Plot (.353 lb TNT 500 ft).

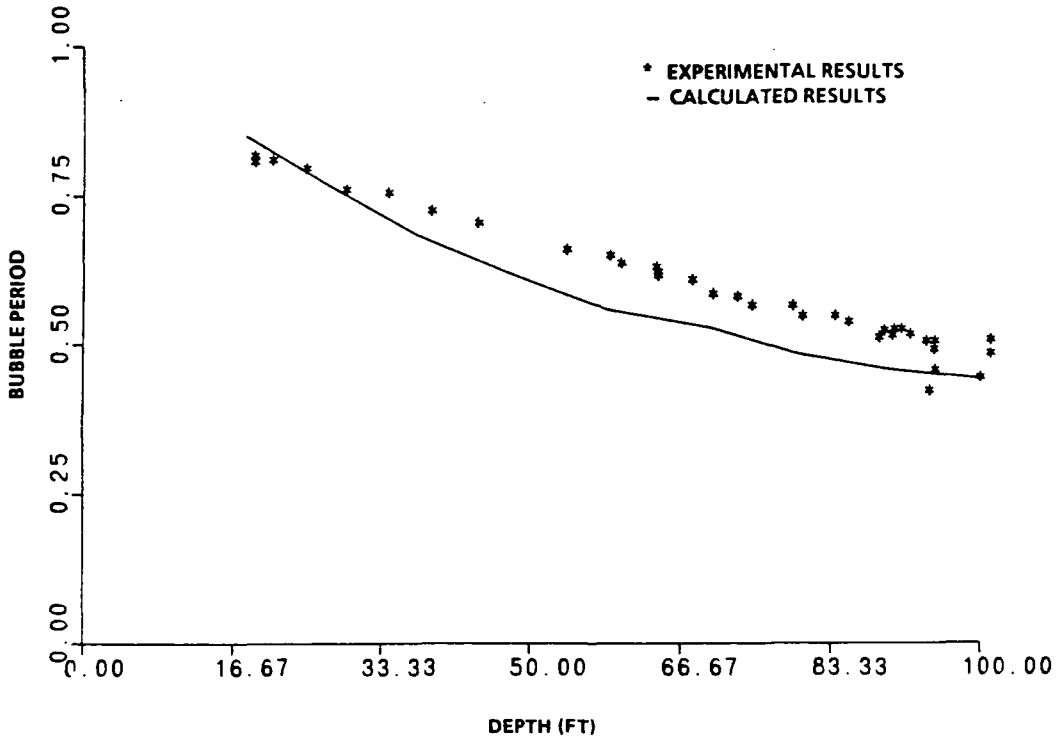

Figure 10. Depth vs. Period Data (300 lb TNT).

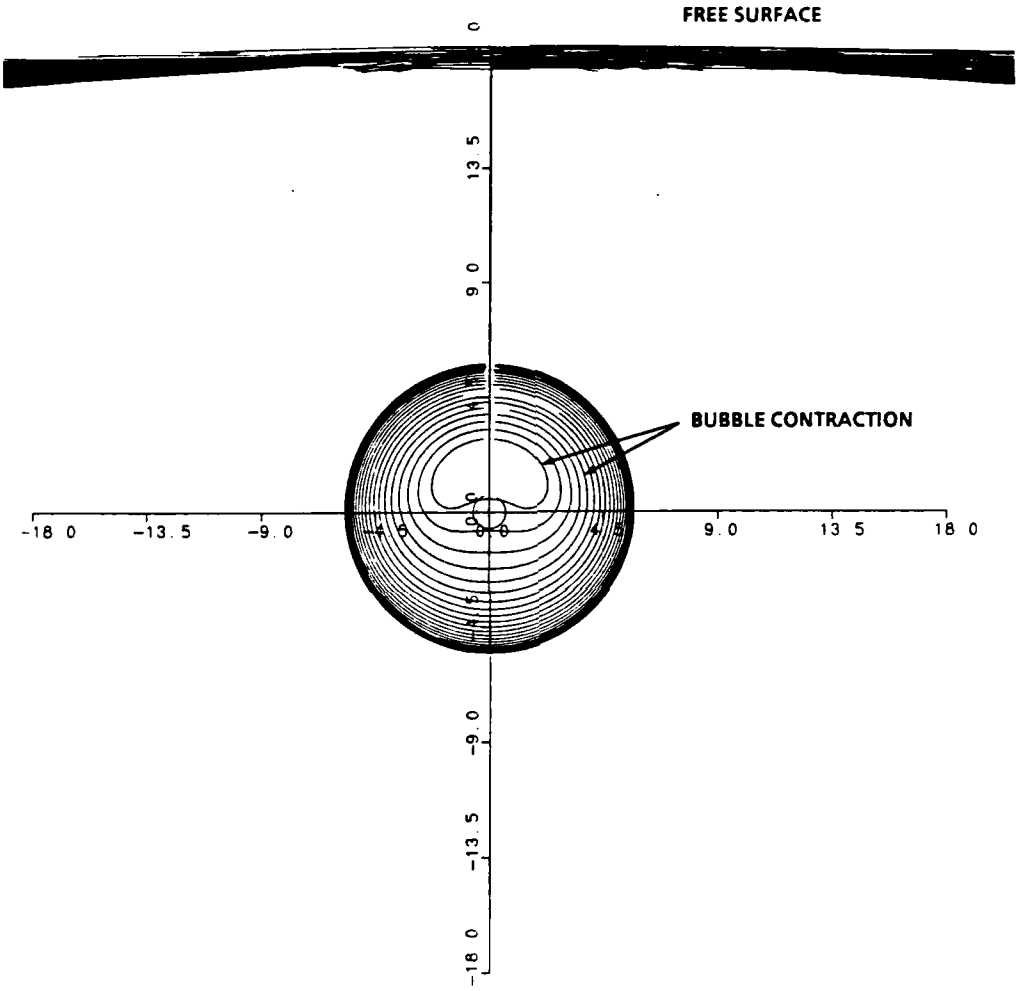

Figure 11. Bubble Profiles (330 lb TNT at 18 m).

USER EVALUATION SHEET/CHANGE OF ADDRESS

This Laboratory undertakes a continuing effort to improve the quality of the reports it publishes. Your comments/answers to the items/questions below will aid us in our efforts.

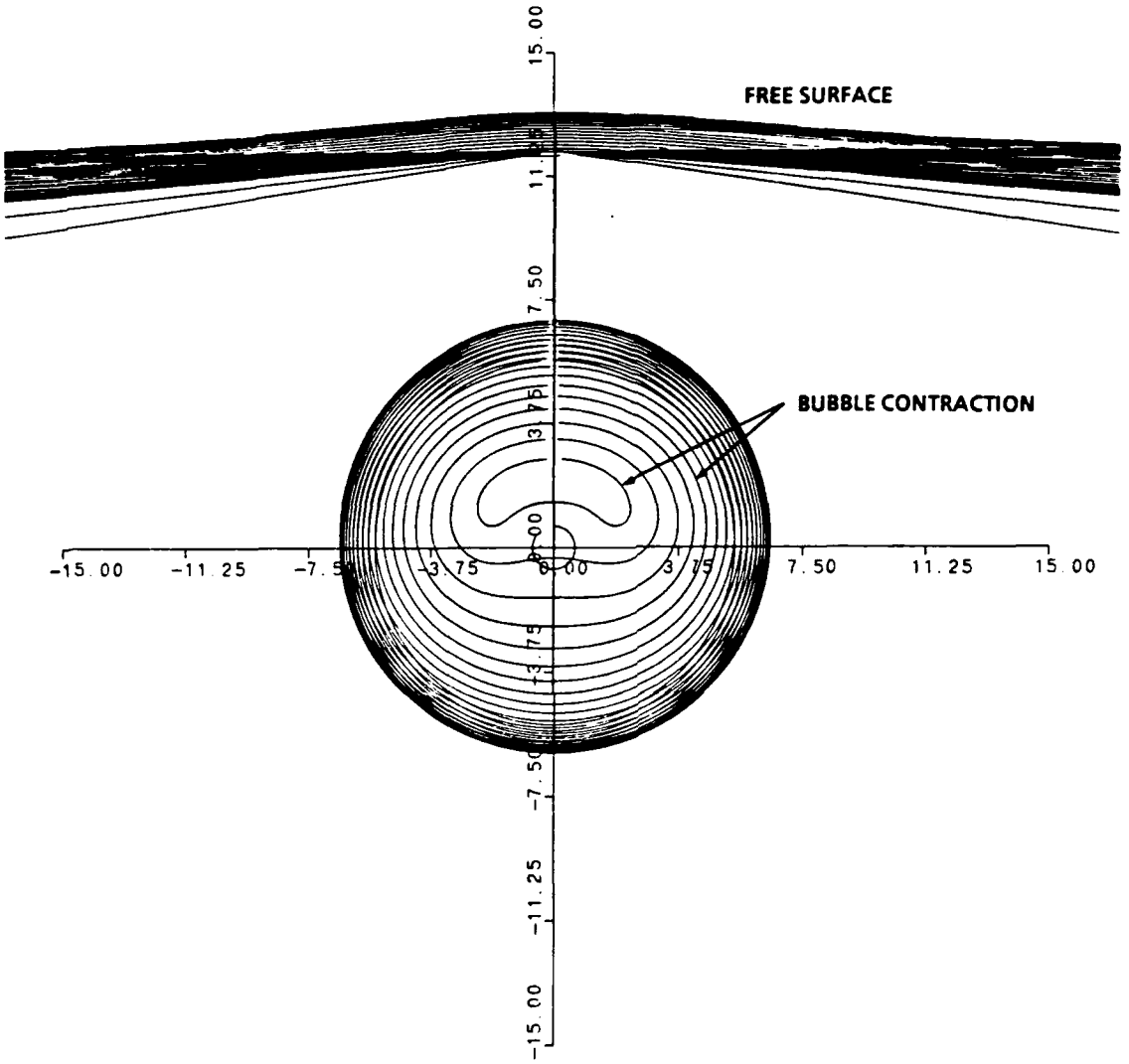

Figure 12. Bubble Profiles (300 lb TNT at 12 m).

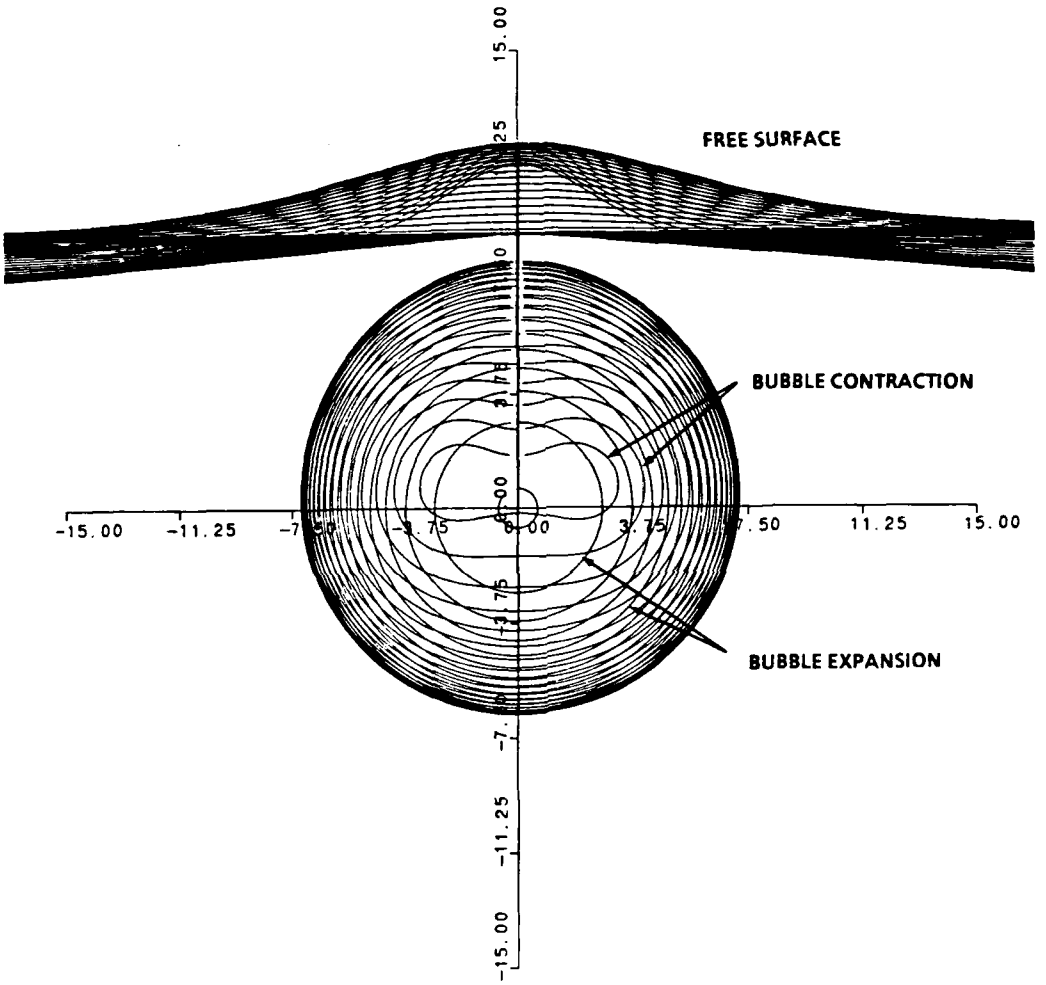

Figure 13. Bubble Profiles (300 lb TNT at 9 m).

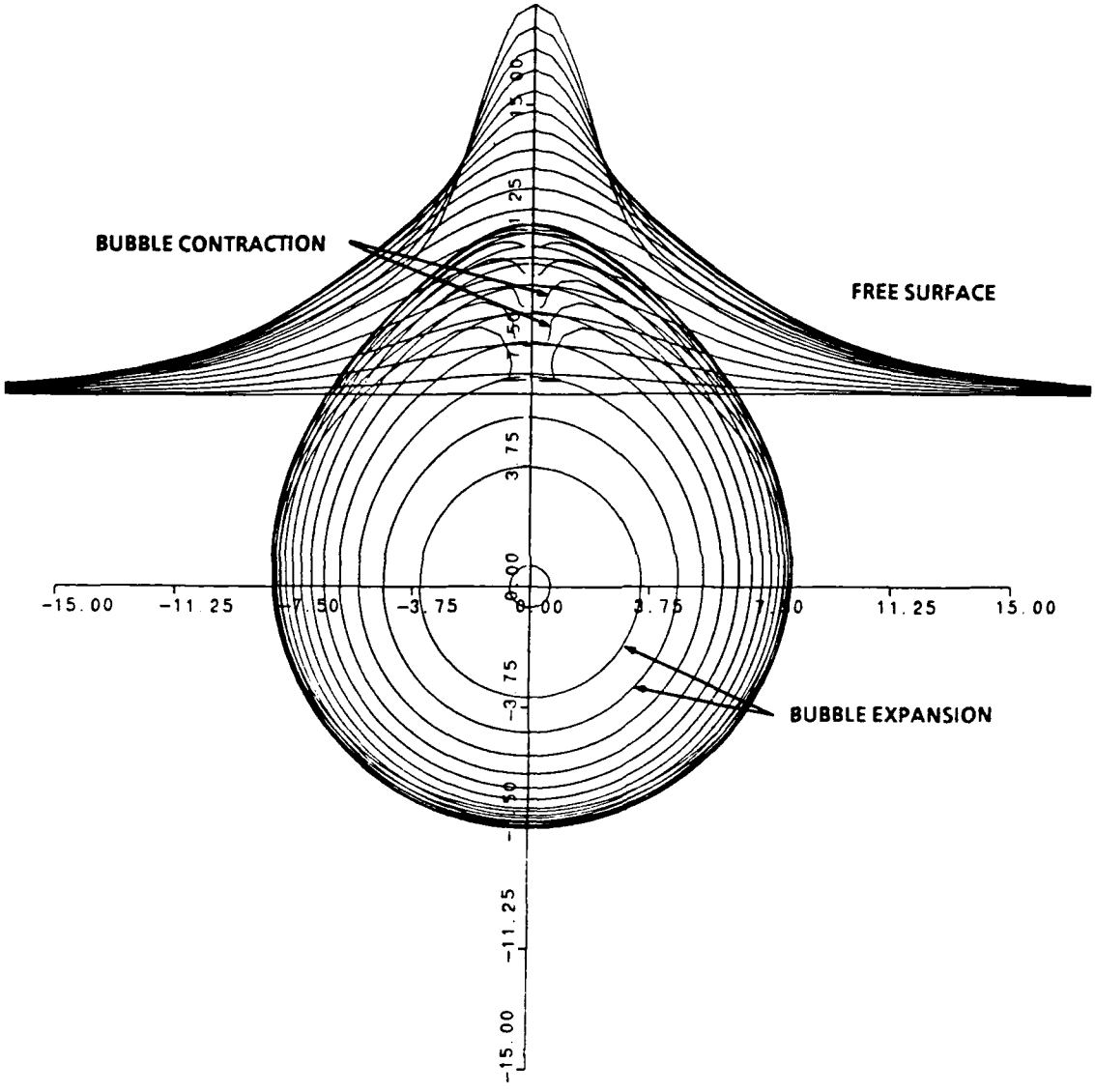

Figure 14. Bubble Profiles (300 lb TNT at 6 m).

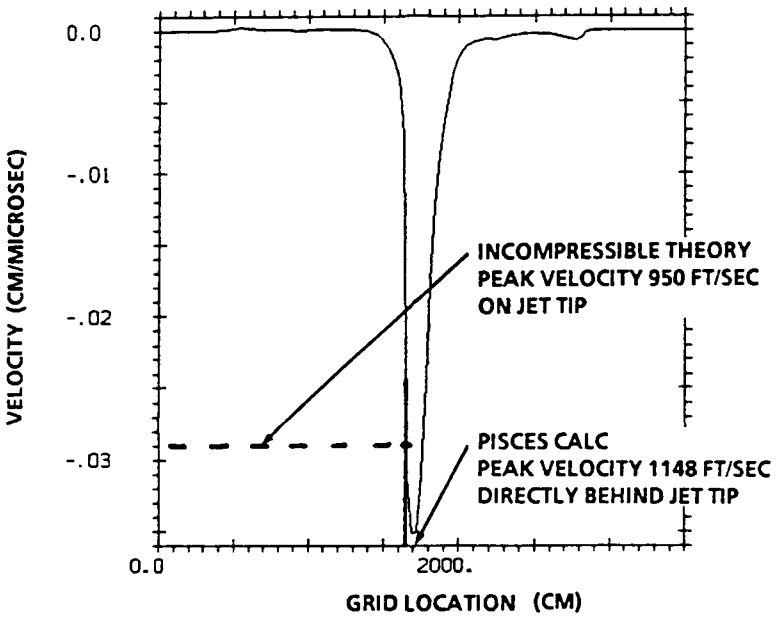

Figure 15. PISCES Calculation for Peak Fluid Velocity (1,200 lb TNT 400-ft Depth).

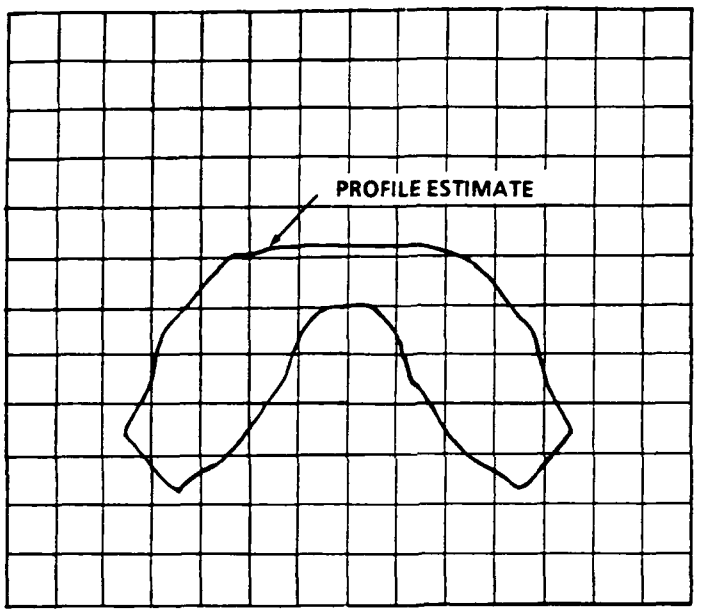

Figure 16. PISCES Calculation for Bubble Profile (1,200 lb TNT 400-ft Depth).

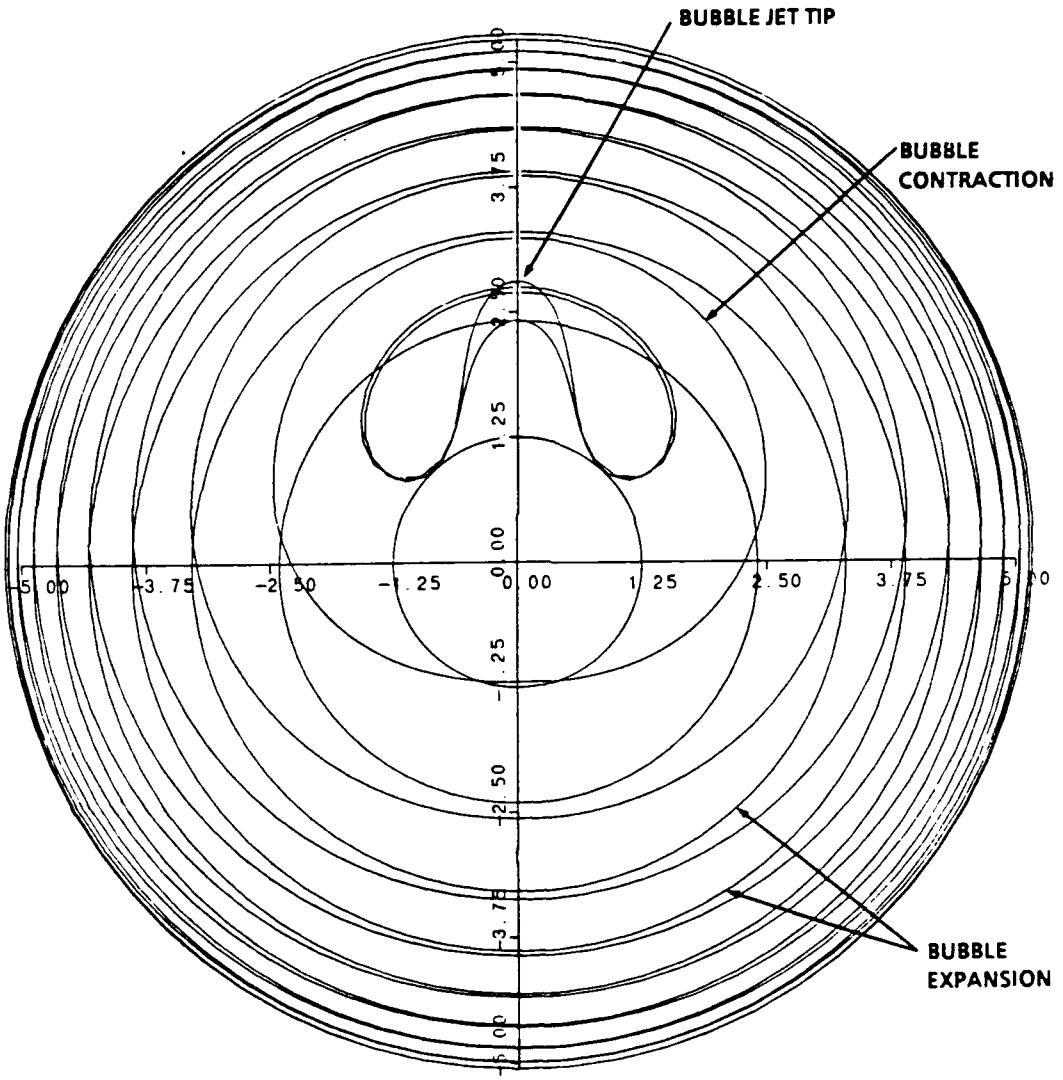

Figure 17. Incompressible Flow Theory for Bubble Profile (1,200 lb TNT 400-ft Depth).

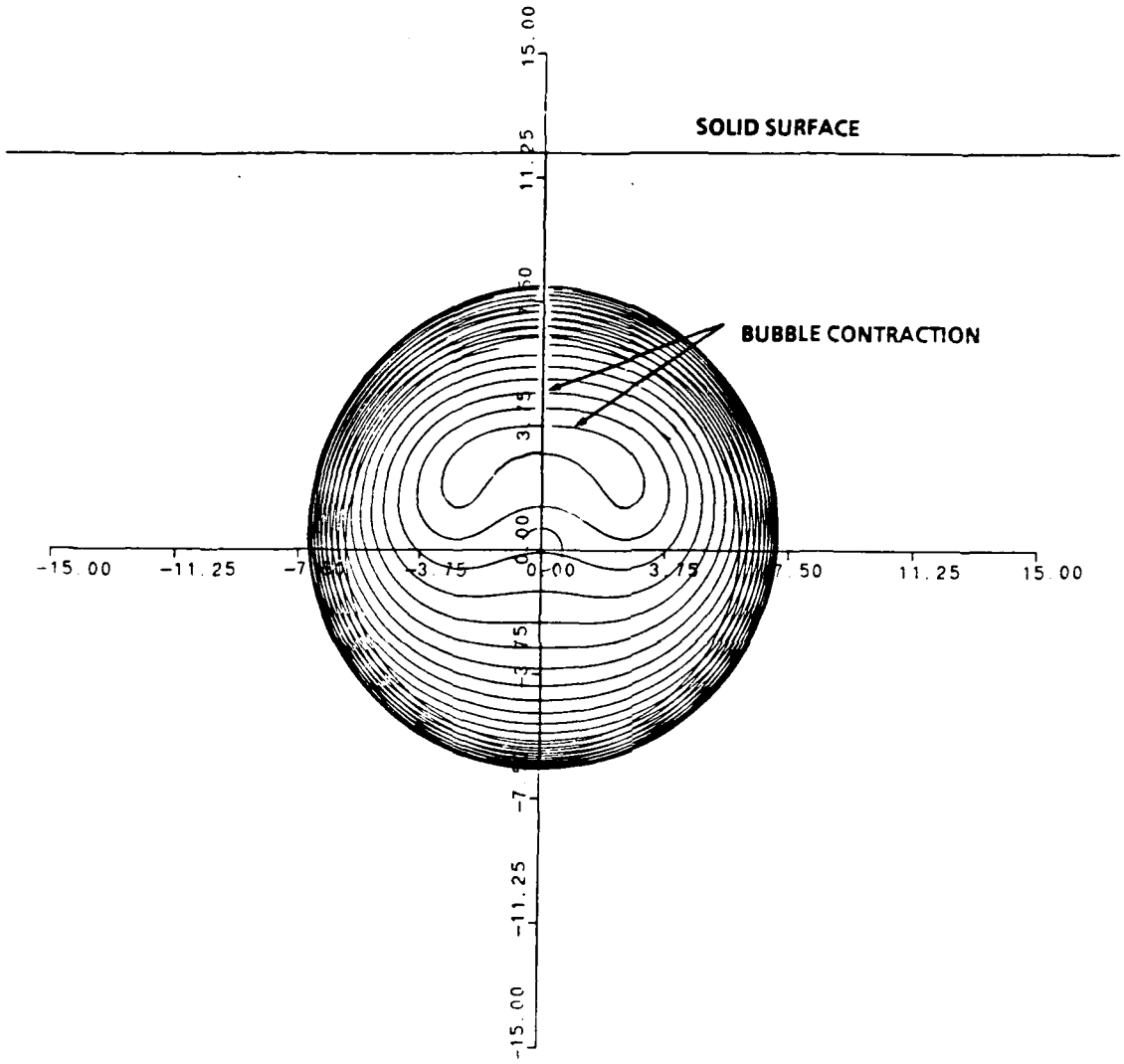

Figure 18. Solid Boundary Calculation (300 lb TNT 12 m).

5. REFERENCES

Chahine, G. L. "Interaction Between an Oscillating Bubble and a Free Surface." American Society of Mechanical Engineers Publication, vol. 77-FE-6, pp. 2–11, 1977.

Chahine, G. L., and A. G. Bovis. "Pressure Field Generated by Nonspherical Bubble Collapse." Journal of Fluid Engineering, vol. 105, no. 3, pp. 356–364, September 1983.

Chahine, G. L., and Ph. F. Genoux. "Collapse of a Cavitating Vortex Ring." Journal of Fluids Engineering, vol. 105, pp. 400–405, December 1983.

Chahine, G. L., Ph. F. Genoux, and H. L. Liu. "Flow Visulation and Numerical Simulation of Cavitating Self-Oscillating Jets." 7th International Symposium on Jet Cutting Technology, Paper A2, pp. 13–32, 26–28 June 1984.

Chahine, G. L., and C. R. Sivian. "Collapse of a Simulated Multibubble System." American Society of Mechanical Engineers Cavitation and Multiphase Flow Form, Albuquerque, NM, 1985.

Chapman, R. B., and M. S. Plesset. "Thermal Effects in the Free Oscillations of Gas Bubbles." Report no. 85–50, Office of Naval Research, June 1970.

Chapman, R B., and M. S. Plesset. "Nonlinear Effects in the Collapse of a Nearly Spherical Cavity in a Liquid." Transactions of the American Society of Mechanical Engineers, pp. 142–146, March 1972.

Cole, R. H. Underwater Explosions. Princeton University Press, NJ, 1948.

Genoux, Ph. F., and C. L. Chahine. "Collapse of a Toroidal Bubble Near a Solid Wall." American Society of Mechanical Engineers Cavitation and Multiphase Flow Form, pp. 69–72, New Orleans, LA, 1984.

Guerri, L., L. Lucca, and A. Prosperetti. "A Numerical Method for the Dynamics of Nonspherical Cavitation Bubbles." Jet Propulsion Laboratory, vol. 82–7, pp. 175–181, 1982.

Johnson, V. E. Jr., et al. "Cavitation and Structured Jets for Mechanical Bits to Increase Drilling Rates." American Society Mechanical Engineers Publication, vol. 82-Pet-13., 1981.

Landau, L. D., and E. M. Lifshitz. Fluid Mechanics, Pergamon Press, Addison-Wesley Publishing Company, Inc., 1959.

Lezzi, A., and A. Prosperetti. "Bubble Dynamics in a Compressible Liquid, Part 2. Second-Order Theory." Journal of Fluid Mechanics, vol. 185, pp. 289–321, 1987.

Prosperetti, A. "Bubble Dynamics: A Review and Some Recent Results." Applied Scientific Research, vol. 38, pp. 145–164, 1982a.

Prosperetti, A. "A Generalization of the Rayleigh Plesset Equation of Bubble Dynamics." Physical Fluids, vol. 25, no. 3, pp. 409–410, March 1982b.

Prosperetti, A. "Bubble Phenomena in Sound Fields, Part Two." Ultrasonics, pp. 115–125, May 1984.

Prosperetti, A. "Physics of Acoustic Cavitation." Frontiers in Physical Acoustics, pp. 145–188, 1986.

Prosperetti, A. "The Equation of Bubble Dynamics in a Compressible Liquid." Physical Fluids, vol. 30, no. 11, pp. 3626–3628, 1987.

Prosperetti, A., and A. U. Jones. "Pressure Forces in Dispersed Two-Phase Flow." Journal of Multiphase Flow, vol. 10, no. 4, pp. 425–444, 1984.

Prosperetti, A., and A. Lezzi. "Bubble Dynamics in a Compressible Liquid, Part 1. First Order Theory." Journal of Fluid Mechanics, vol. 168, pp. 457–478, 1986.

Prosperetti, A., L. A., Crum, and K. W. Commander. "Nonlinear Bubble Dynamics." Journal of the Acoustical Society of America, vol. 83, no. 2, February 1988.

Swift, E. Jr., and J. C. Decius. "Measurement of Bubble Pulse Phenomena, III Radius and Period Studies." The Gas Globe, Underwater Explosions Research, vol. II, ONR, 1950.

Taib, B. B. "Boundary Integral Method Applied to Cavitation Bubble Dynamics." Ph. D. Dissertation, University of Wollongong, Australia, 1985.

Wilkerson, S. A. "A Method for the Calculation of Abscissas and Weight Factors Using Gaussian Integration for Integrans With a Logarithmic Singularity." NSWC TR 87-372, Naval Surface Warfare Center, Silver Spring, MD, 20 November 1987.

No. of Copies	Organization
2	Administrator Defense Technical Info Center ATTN: DTIC-DDA Cameron Station Alexandria, VA 22304-6145
1	Commander U.S. Army Materiel Command ATTN: AMCAM 5001 Eisenhower Ave. Alexandria, VA 22333-0001
1	Director U.S. Army Research Laboratory ATTN: AMSRL-OP-CI-AD, Tech Publishing 2800 Powder Mill Rd. Adelphi, MD 20783-1145
1	Director U.S. Army Research Laboratory ATTN: AMSRL-OP-CI-AD, Records Management 2800 Powder Mill Rd. Adelphi, MD 20783-1145
2	Commander U.S. Army Armament Research, Development, and Engineering Center ATTN: SMCAR-IMI-I Picatinny Arsenal, NJ 07806-5000
2	Commander U.S. Army Armament Research, Development, and Engineering Center ATTN: SMCAR-TDC Picatinny Arsenal, NJ 07806-5000
1	Director Benet Weapons Laboratory U.S. Army Armament Research, Development, and Engineering Center ATTN: SMCAR-CCB-TL Watervliet, NY 12189-4050
1	Director U.S. Army Aviation Research and Technology Activity ATTN: SAVRT-R (Library) M/S 219-3 Ames Research Center Moffett Field, CA 94035-1000

No. of Copies	Organization
1	Commander U.S. Army Missile Command ATTN: AMSMI-RD-CS-R (DOC) Redstone Arsenal, AL 35898-5010
1	Commander U.S. Army Tank-Automotive Command ATTN: AMSTA-JSK (Armor Eng. Br.) Warren, MI 48397-5000
1	Director U.S. Army TRADOC Analysis Command ATTN: ATRC-WSR White Sands Missile Range, NM 88002-5502
1	Commandant U.S. Army Field Artillery School ATTN: ATSF-CSI Ft. Sill, OK 73503-5000
(Class. only) 1	Commandant U.S. Army Infantry School ATTN: ATSH-CD (Security Mgr.) Fort Benning, GA 31905-5660
(Unclass. only) 1	Commandant U.S. Army Infantry School ATTN: ATSH-CD-CSO-OR Fort Benning, GA 31905-5660
1	WL/MNOI Eglin AFB, FL 32542-5000
	Aberdeen Proving Ground
2	Dir, USAMSAA ATTN: AMXSY-D AMXSY-MP, H. Cohen
1	Cdr, USATECOM ATTN: AMSTE-TC
1	Dir, ERDEC ATTN: SCBRD-RT
1	Cdr, CBDA ATTN: AMSCB-CII
1	Dir, USARL ATTN: AMSRL-SL-I
10	Dir, USARL ATTN: AMSRL-OP-CI-B (Tech Lib)

No. of Copies	Organization
1	Commander U.S. Army Missile Command ATTN: AMSMI-RD, W. McCorkle Redstone Arsenal, AL 35898-5010
1	Commander Watervliet Arsenal ATTN: SMCWV-QA-QS, K. Insco Watervliet, NY 12189-4050
3	Commander U.S. Army Armament Research, Development, and Engineering Center SMCAR-FSA-M, R. Botticelli F. Diorio SMCAR-FSA, C. Spinelli Picatinny Arsenal, NJ 07806-5000
2	PEO-Armaments ATTN: SFAE-AR-PM, D. Adams T. McWilliams Picatinny Arsenal, NJ 07806-5000
2	Director Materials Technology Laboratory ATTN: SLCMT-MEC, B. Halpin T. Chou Watertown, MA 02172-0001
8	Director Benet Weapons Laboratory U.S. Army Armament Research, Development, and Engineering Center ATTN: SMCAR-CCB, G. D'Andrea J. Keane T. Allen J. Vasilakis G. Friar J. Zweig L. Johnson T. Simkins Watervliet, NY 12189-5000

No. of Copies	Organization
7	Commander U.S. Army Armament Research, Development, and Engineering Center ATTN: SMCAR-CCH-T, S. Musalli P. Christian K. Fehsal SMCAR-CCH-V, E. Fennell SMCAR-CCH, J. DeLorenzo SMCAR-CC, R. Price J. Hedderich Picatinny Arsenal, NJ 07806-5000
2	Commander U.S. Army Armament Research, Development, and Engineering Center ATTN: SMCAR-TD, M. Linder T. Davidson Picatinny Arsenal, NJ 07806-5000
1	Commander Production Base Mod. Agency U.S. Army Armament Research, Development, and Engineering Center ATTN: AMSMC-PBM-K Picatinny Arsenal, NJ 07806-5000
6	Project Manager Tank Main Armament Systems ATTN: SFAE-AR-TMA, COL Hartline SFAE-AR-TMA-MD, C. Kimker W. Lang SFAE-AR-TMA-ME, K. Russell H. Yuen D. Guzowitz Picatinny Arsenal, NJ 07806-5000
4	Director Lawrence Livermore National Laboratory ATTN: R. Christensen W. Feng F. Magness S. deTeresa P.O. Box 808 Livermore, CA 94550

No. of Copies	Organization
2	Pacific Northwest Lab A Division of Batelle Memorial Inst. ATTN: M. Smith M. Garnich P.O. Box 999 Richland, WA 99352
2	Director Los Alamos National Laboratory WX-4 Division, Mail Stop G-787 ATTN: D. Rabern J. Neal P.O. Box 1663 Los Alamos, NM 87545
4	Director Sandia National Laboratory Applied Mechanics Department, Division-8241 ATTN: C. Robinson G. Benedetti K. Perano P. Nielan P.O. Box 969 Livermore, CA 94550-0096
2	Institute for Advanced Technology ATTN: T. Kiehne H. Fair 4030-2 W. Braker Lane Austin, TX 78759
2	Olin Corporation Flinchbaugh Division ATTN: E. Steiner B. Stewart P.O. Box 127 Red Lion, PA 17356
1	Olin Corporation ATTN: L. Whitmore 10101 9th Street North St. Petersburg, FL 33702
1	Custom Analytical Engineering Systems, Inc. ATTN: A Alexander Star Route, Box 4A Flintstone, MD 21530

No. of Copies	Organization
3	Alliant Techsystems, Inc. ATTN: C. Candland J. Bode K. Ward 5640 Smetana Drive Minnetonka, MN 55343
2	Chamberlain Manufacturing Corp. Waterloo Facility ATTN: T. Lynch 550 Esther Street P.O. Box 2335 Waterloo, IA 50704
	Aberdeen Proving Ground
17	Dir, USARL ATTN: AMSRL-WT-P, I. May AMSRL-WT-PD, B. Burns W. Drysdale K. Bannister T. Bogetti J. Bender J. Ford R. Murray R. Kirkendall T. Erline D. Hopkins S. Wilkerson C. McCall D. Henry R. Kaste L. Burton J. Tzeng

INTENTIONALLY LEFT BLANK.

USER EVALUATION SHEET/CHANGE OF ADDRESS

This Laboratory undertakes a continuing effort to improve the quality of the reports it publishes. Your comments/answers to the items/questions below will aid us in our efforts.

1. ARL Report Number ARL-TR-184 Date of Report August 1993

2. Date Report Received _____

3. Does this report satisfy a need? (Comment on purpose, related project, or other area of interest for which the report will be used.) _____

4. Specifically, how is the report being used? (Information source, design data, procedure, source of ideas, etc.) _____

5. Has the information in this report led to any quantitative savings as far as man-hours or dollars saved, operating costs avoided, or efficiencies achieved, etc? If so, please elaborate. _____

6. General Comments. What do you think should be changed to improve future reports? (Indicate changes to organization, technical content, format, etc.) _____

CURRENT ADDRESS

_____
Organization

_____
Name

_____
Street or P.O. Box No.

_____
City, State, Zip Code

7. If indicating a Change of Address or Address Correction, please provide the Current or Correct address above and the Old or Incorrect address below.

OLD ADDRESS

_____
Organization

_____
Name

_____
Street or P.O. Box No.

_____
City, State, Zip Code

(Remove this sheet, fold as indicated, tape closed, and mail.)

(DO NOT STAPLE)

DEPARTMENT OF THE ARMY

OFFICIAL BUSINESS

BUSINESS REPLY MAIL
FIRST CLASS PERMIT No 0001, APG, MD

Postage will be paid by addressee

Director
U.S. Army Research Laboratory
ATTN: AMSRL-OP-CI-B (Tech Lib)
Aberdeen Proving Ground, MD 21005-5066

NO POSTAGE
NECESSARY
IF MAILED
IN THE
UNITED STATES